A Wavelet Transform Technique for Removing Airplane Echoes from ST Radar Signals

J.-C. BOISSE, V. KLAUS, AND J.-P. AUBAGNAC

Météo-France—CNRM/GMEI/STM, Toulouse, France

(Manuscript received 30 July 1997, in final form 14 May 1998)

ABSTRACT

This paper presents a new technique based on the wavelet transforms for removing airplane and other transitory echoes in strato–tropospheric (ST) radar measurements. This technique provides a time–frequency display of the time series, which is necessary for discriminating the nearly continuous wind signal from transitory pollution such as airplane echoes. Very encouraging results obtained with the VHF INSU/Météo ST radar located at CNRM/Toulouse have shown practical possibilities for a real-time implementation and for applications related to frequency domain interferometry.

1. Introduction

Strato–tropospheric (ST) radars provide information about wind and other atmospheric parameters on a broad range of scales (Balsley and Gage 1980). This capability makes them good candidates to fulfill basic needs of both research and operational meteorology (Larsen 1983; Larsen and Röttger 1982; Klaus 1988). To obtain all of these values, one of the main steps in the signal processing is to produce the power spectrum of the echoes returned to the radar as a function of range. This spectrum contains information on various parameters, such as the total received power, the mean Doppler shift of the atmospheric scatterers, and the distribution of velocities around the mean value (spectral width) (Balsley and Gage 1982). On each spectrum, the radial velocity component is measured directly from the Doppler shift of the signal received from the atmospheric turbulence. Unfortunately, when airplanes appear in one of the lobes of the radar antenna, strong spurious echoes can prevent an accurate computation of the radial velocity and may result in significant errors. Classic low-pass filters are efficient when these echoes are located outside the typical range of atmospheric wind speed—that is, -80 to 80 m s^{-1}—but they are not very effective near airports where aircraft, during takeoff or landing, may have small radial velocities. This is particularly the case with the VHF Institut National des Sciences de l'Univers (INSU)/Météo ST radar (Petitdidier et al. 1990) located at Centre National de Recherche de la Météorologie (CNRM)/Toulouse within a few kilometers of two large airports. Consequently, both atmospheric signal and airplane echo are mixed together in the spectral representation and no criterion is available to discriminate the signals, as is shown in Fig. 1, for example. So we have shifted our attention to time series in order to find any possible method of filtering based mostly on time characteristics of each of those signals. Figure 2 gives typical examples of aircraft echoes on time series selected among a very large database. Noticing particular patterns in such echoes, we investigate the capabilities provided by a time–frequency analysis using wavelet transforms to remove them from the time series before a spectral analysis.

2. Statement of the problem

Examples of aircraft echo pollution are quite numerous with the ST radar in Toulouse. They appear on the time series as strong transitory signals with large frequency variations and amplitude (Fig. 3). These time characteristics make them quite disturbing in the frequency representation (Fig. 4). Unfortunately, low-pass filtering is not very efficient because part of these echoes, the most powerful one in fact, lies within the radial velocity scale of the wind speed. Such has been our experience with the INSU/Météo VHF ST radar located at Centre National de Recherche Météorologiques in Toulouse at close range to the international airport and an important military air base. The given examples show a pollution that affects the radar measurement at a wide scale of range gates given that the radar receives the aircrafts' echoes when they land and take off in the

Corresponding author address: Dr. Vladislav Klaus, CNRM/GMEI/STM, 42, avenue Gaspard Coriolis, 31057 Toulouse Cedex, France.
E-mail: vladislav.klaus@meteo.fr

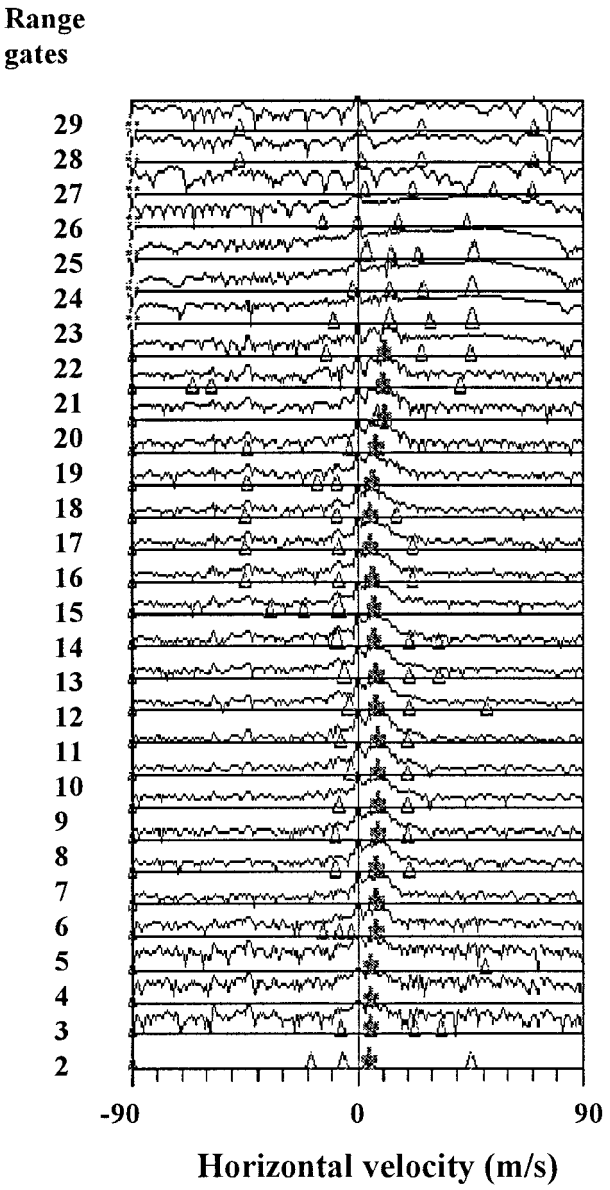

FIG. 1. Example of a spectra profile polluted by airplane echoes during measurements made with the INSU/Météo ST radar at CNRM/Toulouse on 21 August 1996. In each of the 29 range gates, the cross indicates the location of the selected signal, and the triangles show other signal locations.

secondary lobes of the antennas. To give a general idea of the frequency of such pollution, the civil air traffic at the airport is roughly 50 landings and departures per day. This is the most sensitive in the early morning and late afternoon.

The military air base traffic is not published, but experience has shown unpredictable high traffic periods impeding reliable continuous wind measurements. In France, meteorological offices and radio sounding stations are generally located near airports, which means that future projects of installing wind profilers as operational tools for the Weather World Wake will depend largely on the capabilities of such instruments to work efficiently in an intense air traffic environment. The first step in our investigation is a general study of the aircraft echoes on the time series leading to a realistic simulation.

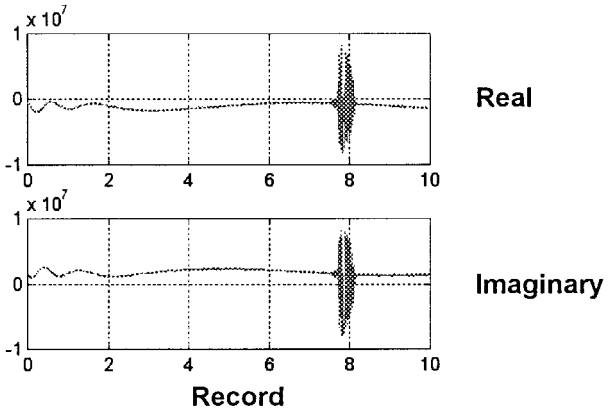

FIG. 2. Time series at the 27th range gate showing airplane pollution around the 8th record.

3. General form of airplane echoes

First, we check whether the aircraft echoes show a general pattern easy to model in our attempt to remove them from the time series. The very form of these echoes is easy to understand if we consider the following scheme of an aircraft passing above the radar.

We consider an airplane with a constant speed V_a flying linearly at a given altitude R above an ST radar. Simulating such an echo in the time series is quite easy (Fig. 5). It includes calculation of both the Doppler frequency and the amplitude of the returned signal according to the time.

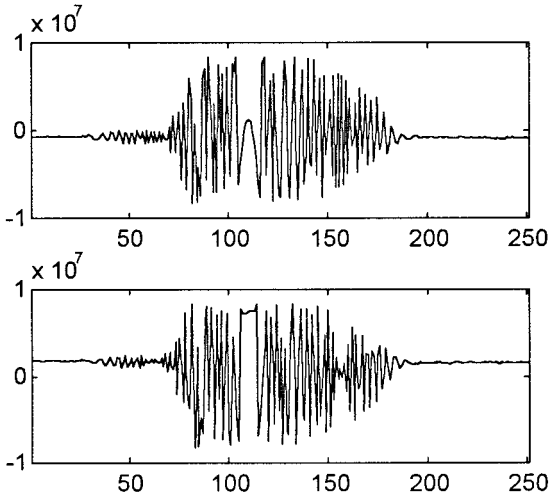

FIG. 3. Same time series as in Fig. 2, zoomed around the spurious echo.

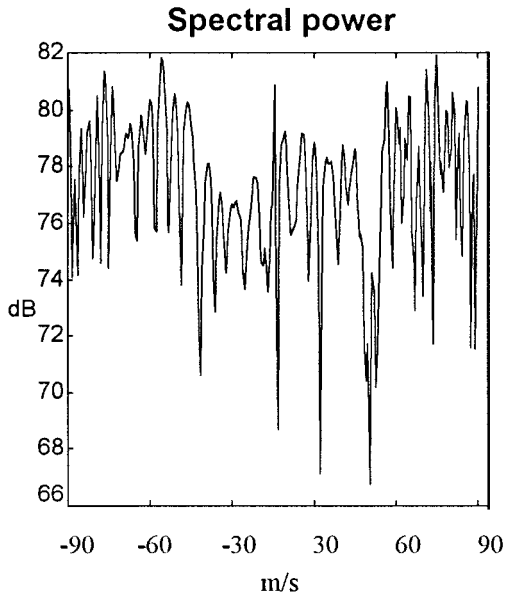

FIG. 4. Spectrum of the polluted part of the time series where the wind signal is totally hidden.

The coordinates (X_a, Y_a) of the airplane relative to the x–y axes depend on time t as follows:

$$X_a = V_a(t_0 - t)$$

$$Y_a = R,$$

where t_0 represents the time when the airplane is just above the radar,

$$\theta(t) = \arctan\left[\frac{V_a(t_0 - t)}{R}\right].$$

The relative velocity of the aircraft seen from the radar is

$$V_r(t) = V_a \sin\theta(t),$$

which gives the Doppler frequency

$$f_d(t) = 2\frac{V_r(t)}{\lambda} = 2\frac{V_a}{\lambda}\sin\theta(t).$$

The amplitude of the echo is computed assuming no variation in the reflectivity of the airplane. This assumption seems rather crude, but at this step we look mainly for a general pattern that could apply to any kind of aircraft. We shall see in section 5 that wavelet matching does not need to be perfect in this matter for an efficient filtering. This radar is equipped with an antenna gain $G(\theta)$ equating approximately a sine function because the transmittting energy is equally distributed over the antenna. Such a simulation is quite realistic given that the ST radar antenna network is uniformly fed. Previously, with the aid of a helicopter, this was demonstrated effectively with antenna diagram measurements. If ''lobe'' is the antenna main lobe aperture at 3 dB, we get

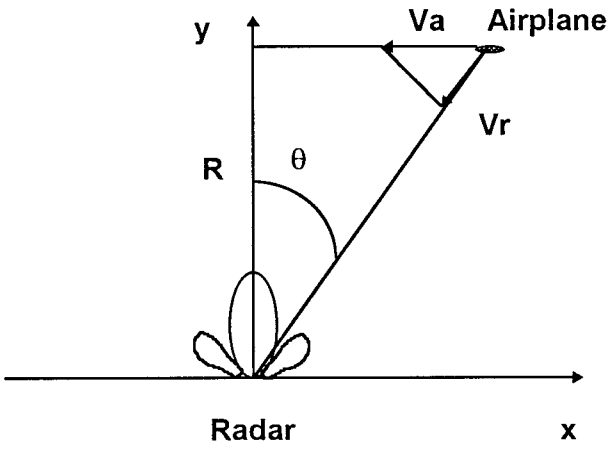

FIG. 5. Schematic view of an airplane flying above an ST radar system.

$$G(\theta) = \text{sinc}\left(\pi\frac{\theta(t)}{\text{lobe}}\right),$$

which shows that the first angle of minimum reception is at $\theta(t) = \text{lobe}$ from the zenith.

Having both the frequency $f_d(t)$ and the amplitude $G(\theta(t))$, we can write the resulting echo $S(t)$ as follows, considering the real and the imaginary components of the time series:

$$S(t) = G[\theta(t)]\exp 2\pi j f_d(t).$$

Figure 6 shows an example of such simulation using the following values: airplane speed, $V_a = 138$ m s^{-1} (500 km h^{-1}); altitude of the aircraft, $R = 3500$ m; antenna main lobe aperture, lobe = 5°; and time reference, $t_0 = 0$ s. The echoes have a particular pattern that shows variations in amplitude, according to the antenna lobes, and in frequency, depending on the radial

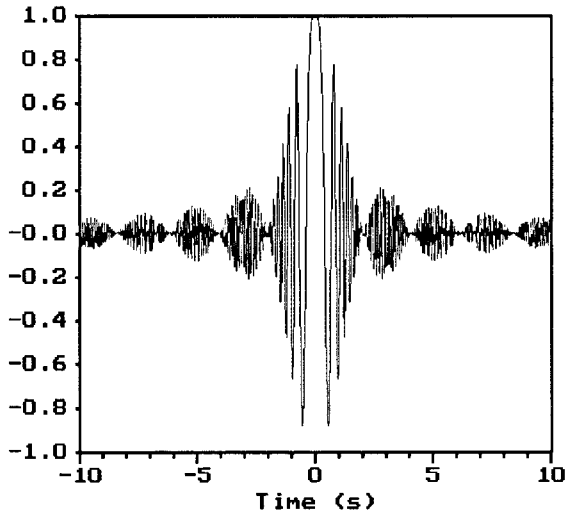

FIG. 6. Simulated airplane echo signature on a time series for a vertical beam antenna.

velocity relative to the radar. The effective measurements confirm the validity of the assumptions used for this simulation. Having found a general pattern, we use a wavelet filtering to remove echoes from the time series.

4. Wavelet transforms principle

The applications of wavelet transforms are already used in oceanic and atmospheric science. Currently, they are successfully implemented in oceanic (Liu and Miller 1996) and atmospheric studies (Weng and Lau 1994). For wind profiler signal processing, work has already been done in the removal of the ground clutter (Jordan and Lataitis 1997). In this case, the authors use the wavelet transform for filtering the slowly varying ground clutter relative to the faster clear-air return. We consider the same type of problem but in an exactly opposite sense. The clear-air return is much smoother than the aircraft echo we want to remove. So the principle is the same, but the methodology will be quite different.

The wavelet transform is a way of expressing a signal through a convolution by a certain number of basic functions called ''wavelets'' (Strang and Nguyen 1996). These basic functions have a fundamental pattern called the ''mother wavelet'' $\psi(t)$, giving rise to a family of daughter wavelets $\psi[(t - b)/a]/\sqrt{a}$. The parameters a and b denote, respectively, scaling and shifting of the mother function. We can use continuous wavelet transforms with arbitrary a and b, or numerically efficient, discrete wavelet transforms such as a power-of-two sequence (Daubechies 1988):

$$a_j = 2^{-j} \quad \text{and} \quad b_k = k2^{-j},$$

which gives

$$\psi_{j,k}(t) = (2^{j/2})\psi(2^j t - k).$$

Here j and k denote, respectively, the level that can be related to the frequency and the time location of the wavelet. The zero level is selected for a scale matching the length of the record. As we shall see further, only the fourth and eighth levels will be used to detect and remove airplane echoes from the ST radar time series.

For a signal $x(t)$, the wavelet transform is expressed as

$$C_x(a, b) = \frac{1}{\sqrt{a}} \int_{-\infty}^{+\infty} x(t)\psi^*\left(\frac{t - b}{a}\right) dt. \qquad (1)$$

Each coefficient indicates whether a particular level related to a is present at a certain time centered at b. Here, ψ is the mother wavelet, ψ^* its complex conjugate, a the level, and b the time. The (b, a) plane is called the ''time-level plane.'' The initial signal $x(t)$ can then be rebuilt from the wavelet coefficients according to

$$x(t) = \frac{1}{K} \int_a \int_b C_x(a, b)\Psi_{a,\,b}(t) \frac{da\ db}{a^2}, \qquad (2)$$

where

$$K = \int_{-\infty}^{+\infty} \frac{|\Psi(\nu)|^2}{|\nu|} d\nu$$

and

$$\psi(t) \xrightarrow{\text{Fourier Transform}} \Psi(\nu).$$

5. Choice of a wavelet basis function for airplane filtering

Considering the wavelet transform expression (1), we notice a strong analogy with the correlation function between $x(t)$ and another signal $y(t)$ having finite energy:

$$C_{xy}(\tau) = \int_{-\infty}^{+\infty} x(t)y^*(t - \tau)\, dt. \qquad (3)$$

That means the wavelet coefficients will be the highest if we choose a wavelet of the same pattern as the signal we try to detect. In this way, we build a family of functions that allows an optimum detection of the airplane echoes. To this end, we choose a wavelet whose basic equation is

$$\psi(t) = \begin{cases} G(\theta)\cos(2\pi f_d t), & \text{if } \theta \in [\text{lb, lh}] \\ 0, & \text{otherwise,} \end{cases} \qquad (4)$$

where

$$G(\theta) = \left|\text{sinc}\left(\frac{\theta}{\text{lobe}} - \theta_0\right)\right|,$$

$$\theta(t) = \arctan\left(\frac{V_a t}{R}\right),$$

$$f_d = \frac{2V_a f_r \sin(\alpha)}{c},$$

$$\alpha = \theta + \sin(\theta)\theta_1,$$

$$\text{lb} = \text{lobe} - \theta_0, \quad \text{and}$$

$$\text{lh} = -\text{lb}.$$

In (4), ψ includes six parameters that are f_r, the radar transmitter frequency; θ_1, a corrective term that regulates the minimum Doppler frequency of the central part of the wavelet; and θ_0, the possible asymmetry of ψ (if $\theta_0 = 0$, then the function ψ is symmetric). The terms V_a, R, and lobe have already been defined.

In this equation, we notice that V_a and f_r determine the maximum frequency of ψ on its interval [lb, lh], and lobe and R influence the interval [lb, lh] through the V_a/R ratio.

Some examples of wavelets belonging to this family are given in Fig. 7. We notice a close analogy with the simulated airplane echo given in Fig. 6 because we use the same antenna diagram $G(\theta)$. For practical purposes, a symmetric wavelet has been chosen, which is the best compromise between measurements obtained from two opposite oblique beams, such as north and south or east

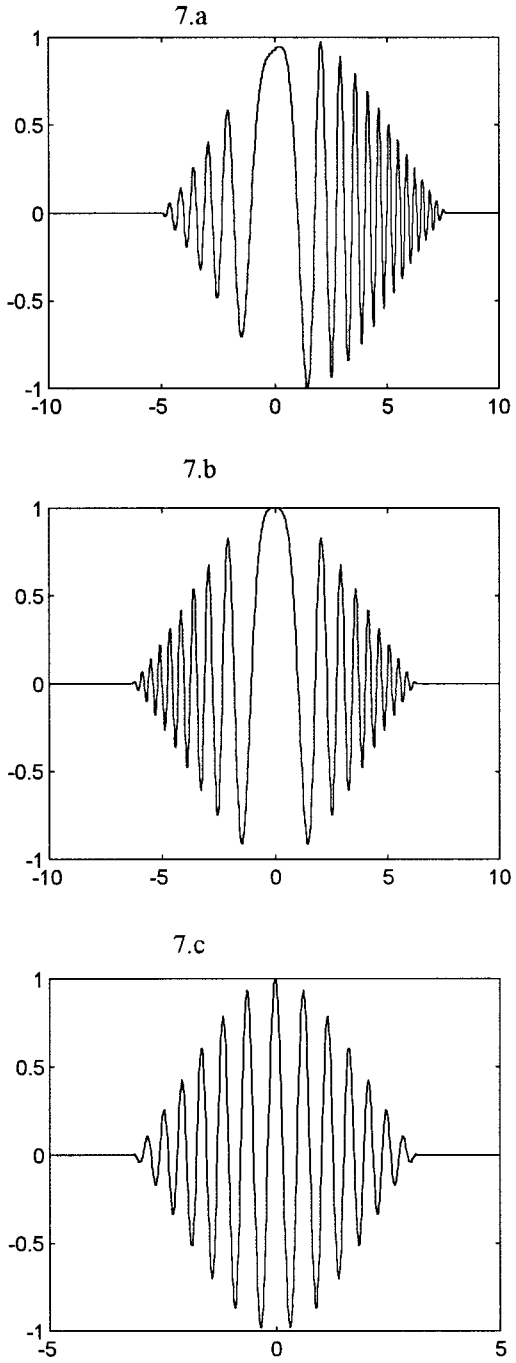

FIG. 7. Examples of wavelet patterns chosen for airplane echoes filtering in the time series.

and west. The symmetric wavelet that has been used has the following characteristics. The parameter V_a's value is 55.5, R is 4000, θ_1 is $\pi/36$, θ_0 is 0, f_r is 45×10^{-6}, and lobe is $\pi/72$. We can check if such a function satisfies the definition of a wavelet; that is,

$$\int_{-\infty}^{+\infty} \psi(t)\, dt = 0 \quad \text{and} \quad \int_{-\infty}^{+\infty} |\psi(t)|^2\, dt = 1.$$

A numerical computation has given, respectively, 0.16 and 1.43, which shows a slight discrepancy from the theoretical values. These differences are not very important, because here the wavelet transform will be used only for detection and removal of polluted parts of the time series.

In their wavelet filtering to reduce ground clutter, Jordan and Lataitis (1998) use a classic Daubechies 20 wavelet (Daubechies 1988; Newland 1994) for computing the whole set of wavelet coefficients from the time series. Then, after limiting coefficients under a threshold value, they rebuild the entire time series from the wavelet coefficients. In such computation, the above assumptions are absolutely necessary in order to preserve the energy balance of the signal.

The second important difference from the method of Jordan and Lataitis (1997) lies in the fact we use only two levels of wavelets, as described herein.

6. Application to spectral processing

a. Signal processing

The wavelet coefficients are calculated through expression (1). Having defined the mother wavelet function, we can proceed to time series processing. The automatic filtering operates according to the architecture presented in Fig. 8. The following rules have been applied.

- At the beginning of processing, when starting the radar, we calculate the maximum value of the wavelet coefficients for the first three time series provided by the radar. The lowest of these values becomes the reference level. Then, if a time series has a wavelet coefficient at least 10 times higher than this reference value, a spurious echo is considered present. If the highest wavelet coefficient is less than the reference value, it becomes the reference value.
- We compute the wavelet transform for levels 4 and 8. That means we convolute the time series, with the following functions directly deduced from (4):

  level 4 $\quad \psi(t) = 4G[\theta(16t)] \cos[2\pi f_d(16t)]$

  and level 8 $\quad \psi(t) = 16G[\theta(64t)] \cos[2\pi f_d(64t)]$.

  Thus, each point of the times series corresponds to one coefficient obtained from a convolution with the level-4 wavelet and one coefficient from a convolution with the level-8 wavelet.
- When any coefficient is 10 times higher than the reference level, we eliminate the part of the time series consisting of 80 points on each side of the corresponding point. This number has been empirically deduced from experience.
- When a spurious echo has been detected in the range gate N, the three adjacent range gates below and above are also considered polluted. This is deduced from observations of strong aircraft echoes. It may not be

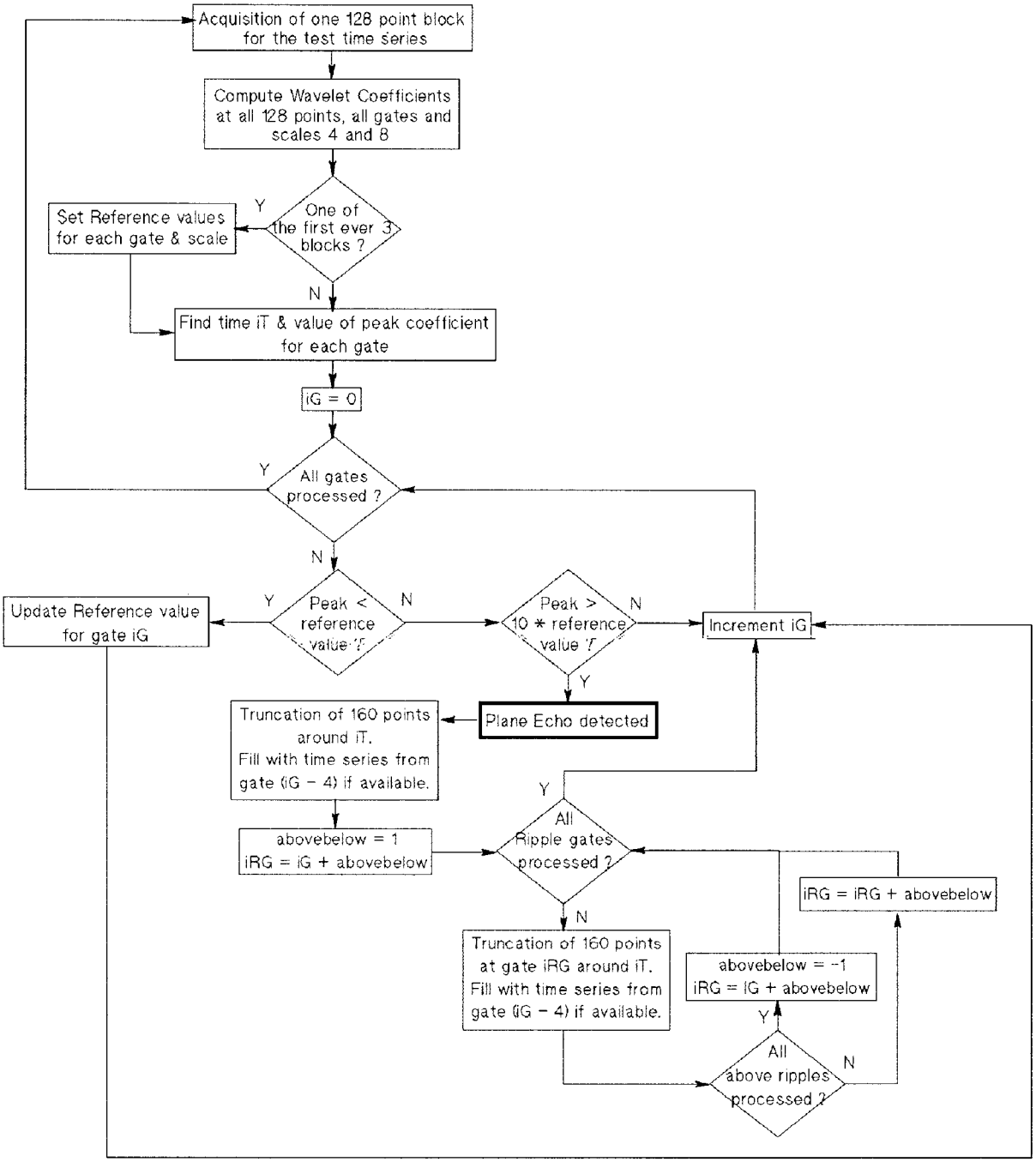

FIG. 8. Flowchart depicting the plane filter module implemented in the spectral processing chain.

the case all of the time when spurious echoes are weaker, but in our attempt to implement an automatic processing for a maximum filtering, we have been inclined to remove these data, whether they are polluted or not.

- If the number of removed points is less than 25% of the total number of the time series, we join both ends and complete the dataset with those from the adjacent time series. If this number is above 25%, we simply remove the time series from further calculation and consider the range gate to be lost. This is not very crucial, as we shall see later.
- Once the time series has been filtered, we calculate the spectrum through a fast Fourier transform using the classic means for retrieving the clear-air signals. As for each range gate, when we obtain a spectrum every 10 or 20 s, it is efficient to use the so-called incoherent integration that sums the successive spectra

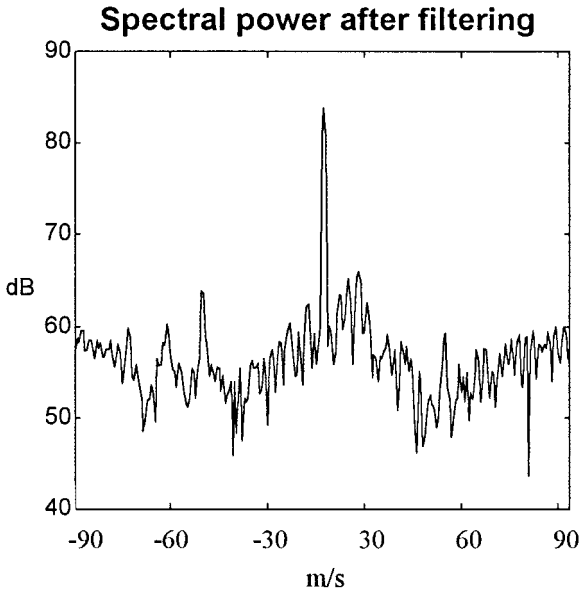

FIG. 9. The same spectrum as in Fig. 4 after wavelet filtering. Some spurious echoes remain, but the wind signal, located around the 25 m s^{-1} abscissa, is easily detectable.

for each range gate in order to reduce the random noise variations for a better detectability of the more deterministic clear-air signal ( ). Typically, with the VHF radar, we compute up to nine successive spectra for each range gate, which allows us to obtain three-dimensional wind profiles every 15 min, which is enough for most scientific and routine observations. Removal of a spectrum from time to time is practically unnoticed in the final wind computation.

This method may still be improved by a complete wavelet reconstruction according to (2), but at this point, we were concerned about processing time: we were trying to develop a technique fast enough to be easily implemented.

b. Application example

Airplane echoes are quite numerous at CNRM/Toulouse, where a VHF INSU/Météo ST radar is located. A typical example is given in Fig. 1, which shows such an occurrence above the 22d range gate. To test the method, we have applied the wavelet transform on the related time series of the radar measurements during a period that included 10 successive records. The wavelet transform has clearly detected aircraft echoes on the last gates around the eighth record, as is indicated in Fig. 2. By zooming around the spurious echo, we find the typical signature of an aircraft (Fig. 3). Of course, in the corresponding spectrum, the wind signal is completely hidden by the airplane echo that covers the entire spectral width. We also notice a mean power of about 76 dB, which prevents any possibility of valid signal detection (Fig. 4).

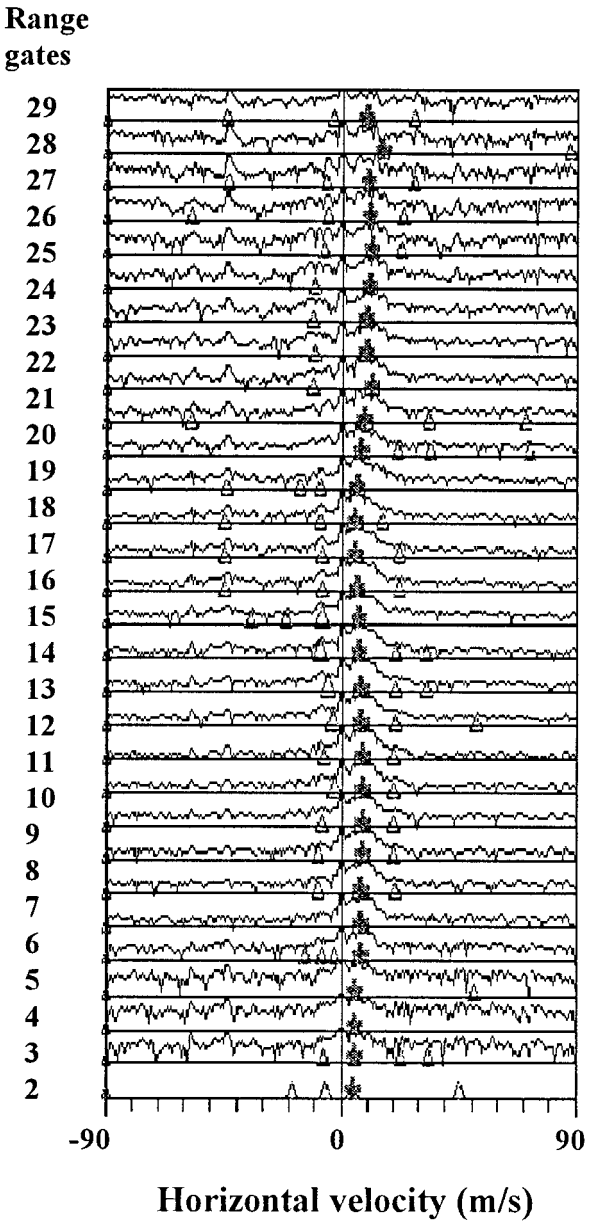

FIG. 10. The same spectra profile as in Fig. 5 after wavelet filtering, allowing removal of airplane echoes above range gate 22.

Using the wavelet transform described above, we remove the high coefficients involved in the airplane echoes and complete the time series with an unpolluted part (see Fig. 9). Hence, the spectrum has been successfully cleaned (Fig. 10). The average level has been reduced by more than 20 dB, showing the efficiency of the wavelet filtering to remove even such a huge spurious signal. Now the wind signal is sufficiently apparent to be detected through the classic methods. Some slight spurious echo signature remains but without any consequences on the measurement quality. All of the polluted range gates have been processed in the same way, allowing a retrieval of the wind signal on the entire profile (Fig. 11).

7. Application to FDI processing

a. Plane filter in the FDI processing chain

The automatic filtering operates according to the flowchart presented in Fig. 11. It runs automatically in the time-delayed analysis of the frequency domain interferometry (FDI) time series.

Here, the extent of the plane echo, the contamination of adjacent gates by ''ripples'' of the echo, and the extent of this contamination are all adaptive. The preliminary testing of a given time series segment is also selective, considering only the largest absolute values of voltage.

Under the current setup of the FDI analysis, the processing modules handle time series units called ''blocks,'' consisting of 128 consecutive points for each frequency. Correlations and spectra are computed over each block and incoherently averaged over four and eight blocks, respectively. One run of the plane filter module covers a period of eight blocks, plus two extra ''buffered'' blocks, one at each end of the period. A single component is tested for the presence of a plane echo, usually the I component for the lowest frequency.

Wavelet coefficient thresholds, or reference values, are set up for each gate over the first three blocks encountered. All points in the blocks are used to compute the thresholds. On the contrary, the preliminary testing of other blocks is limited to the 20 largest absolute values of voltage in each block and gate. The peak wavelet coefficient absolute value is compared to the reference value for the corresponding gate. It may serve to update the reference value or signify that a plane echo is present. Here, a value greater than 10 (60) times the reference value is synonymous of the presence of a type-2 (type-1) plane echo.

The detection of a plane echo at time iT triggers the computation of wavelet coefficients at all points over a 128-point secondary testing window centered at iT. The extent of the plane echo is then determined using a criterion over two running windows starting at iT and moving toward both edges of the secondary testing window. Usually, those running windows are 10 points long, and their outer edge is the end of the plane echo when fewer than 8 points out of 10 show wavelet coefficients larger than three times the reference value.

The detection of a plane echo at time iT also triggers the testing of at most three gates above and below the contaminated gate. The testing starts at the gate adjacent to the polluted gate and progresses in the proper (outward) direction. It stops when the current gate does not show evidence of plane echo ripples. Wavelet coefficients are computed over a 128-point window centered at iT. A peak coefficient larger than six times the reference value for the current gate is necessary for the gate to be considered polluted. The extent of the ripple plane echo is then determined in the same manner as the extent of the plane echo.

Although not specified in the flowchart, the uncontaminated part of the tested block is also tested for the presence of a second and then a third plane echo, and the course of events described above is reproduced. Nontrustworthy points are discarded for detrending and component recalibrating of the time series. They are also discarded from the computation of auto- and cross correlations. When more than half the number of points in a block is contaminated, the whole block is discarded, and the correlations are incoherently integrated over one less block. The behavior is different for the computation of auto- and cross spectra. The detrending and recalibration module attempts to reconstruct segments of 128 consecutive uncontaminated points, using points from the adjacent blocks. The two buffered blocks at the ends of the eight-block period tested by the plane filter module allow such a reconstruction when the first or last block is affected. When more than half of the points in a block are contaminated, the whole block is discarded, and the spectra are integrated over one less block. The use of a Hanning window prior to the FFT computation and the discarding policy ensures that the spectra used in the integration are not redundant.

b. Application examples

The time-delayed analysis of the FDI time series, as opposed to real-time wind calculations, was a less stringent environment for the adaptation of the airplane echo detection technique.

In the FDI configuration, the radar scans alternatively each beam direction with two closely spaced frequencies, providing two interleaved time series records. The cross correlation of the series or, alternatively, of their Fourier transforms, serves to test the presence of an isolated scattering layer within each resolution volume, and, if so, documents the position and width of the layer. The FDI information is highly gate specific and prevents us from substituting time series segments from adjacent gates for plane-polluted segments. The transitions between these copied segments and the unpolluted time series may also be detrimental to the cross-correlation and cross-spectrum parameters.

Figure 12 illustrates the effect of the plane echo eradication on the autospectrum for two gates collected in a oblique beam on 15 December 1997. The left graph shows in a gray shade the proportion of points in the eight-block period affected by the plane echo. The top and middle graphs show the lowest frequency I component time series record, respectively, before and after the echo eradication. Shaded times are considered affected, and shaded lozenges between the graphs indicate the provenance of the reconstructed sets. The two bottom graphs show the power spectra before (left) and after (right) the eradication. The effect is dramatic in this oblique beam record and at these signal altitudes. The folded plane echo peak would have seriously impaired the normalization of the cross spectra and, therefore, the FDI information.

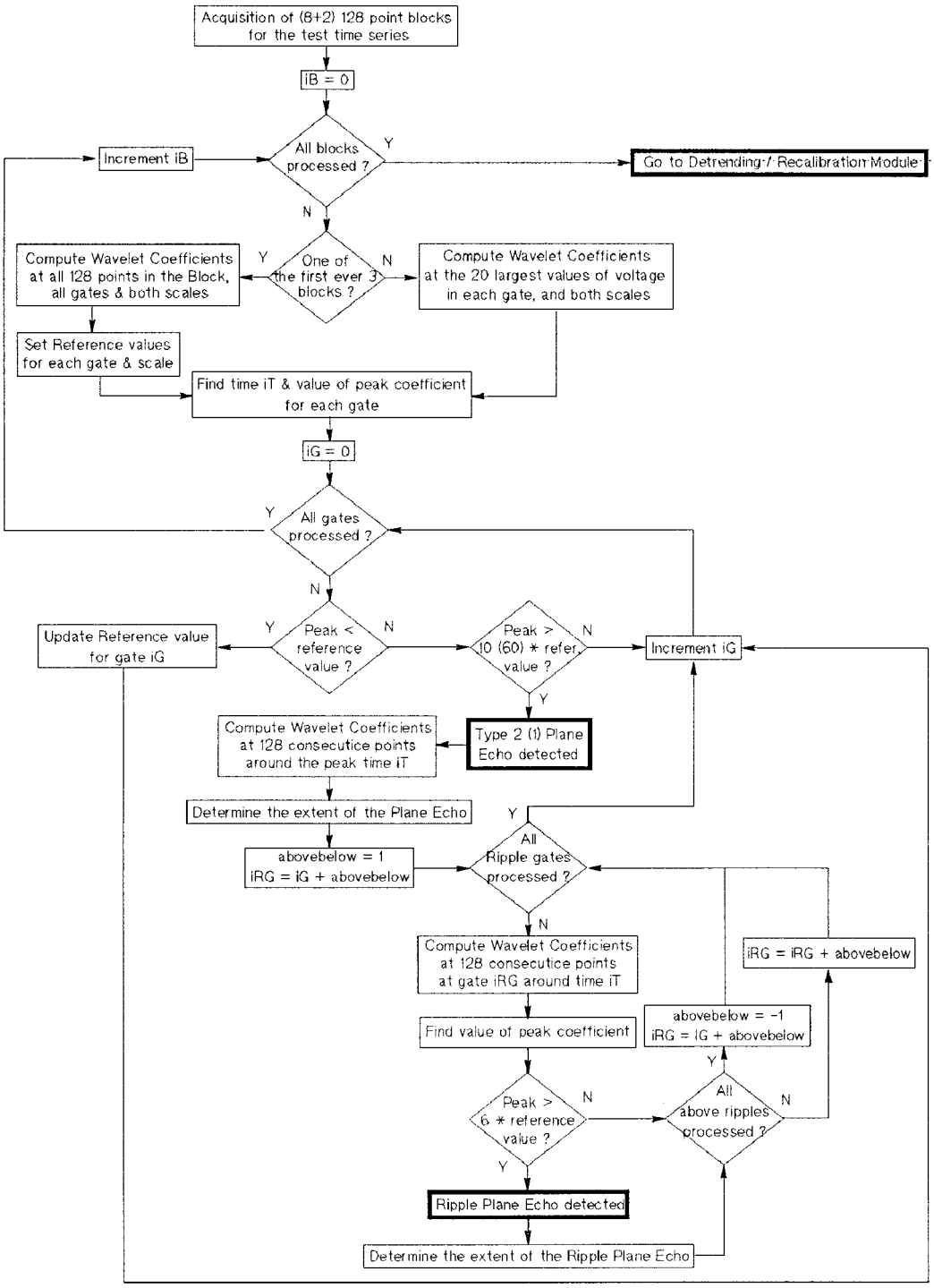

FIG. 11. Flowchart depicting the plane filter module implemented in the FDI processing chain.

Figure 13 is similar to Fig. 12 except that the plane echo is detected here at high altitudes in a vertical beam on 20 August 1996. The figure illustrates the ability of the technique to detect multiple closely spaced echoes, inducing here an incoherent integration limited to six blocks. Little signal is, however, present at these gates, and the effect on power spectra is less straightforward.

Last, Fig. 14 shows the effect of a plane echo on the correlation parameters over two successive four-block periods for the same gate and for an oblique beam on

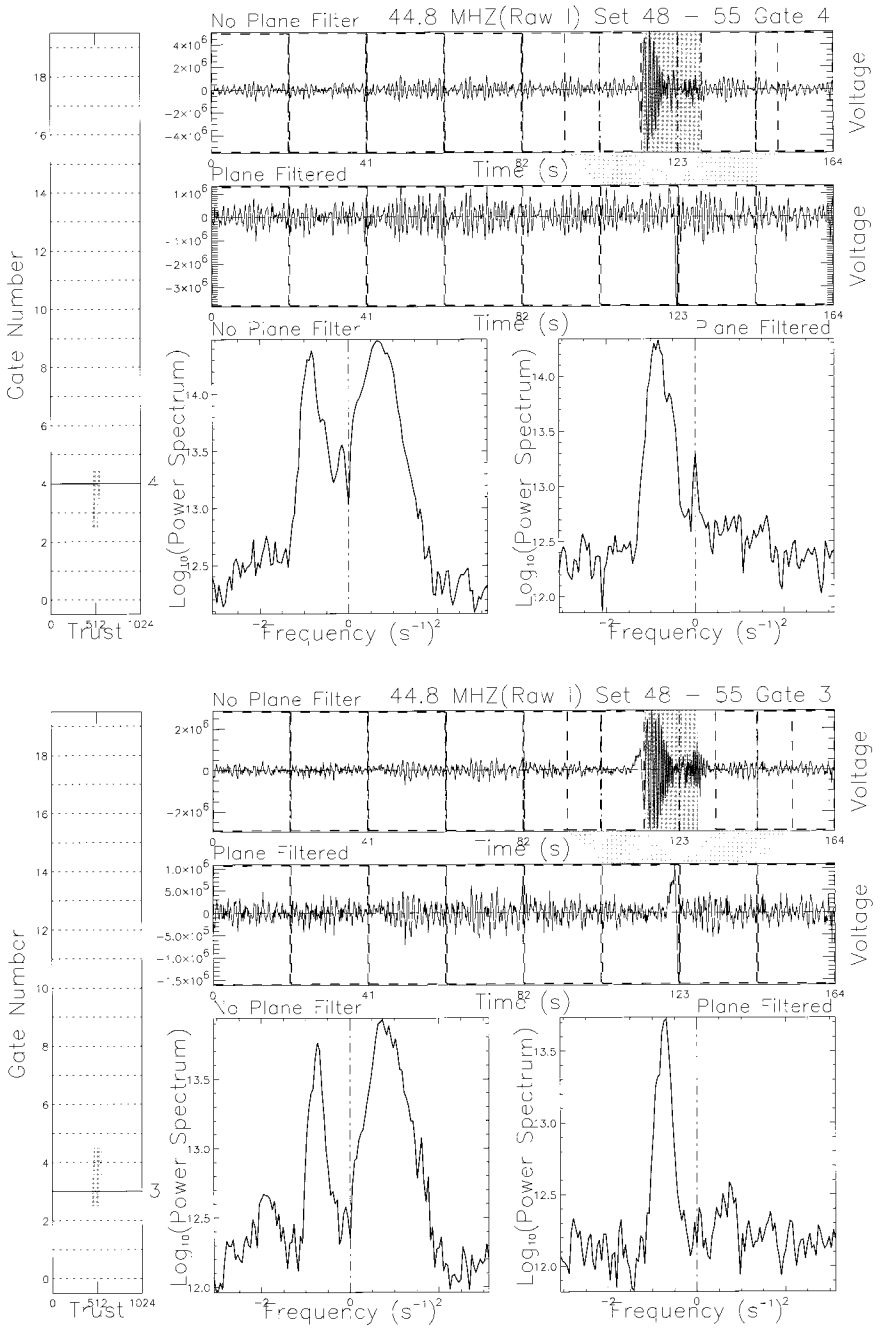

FIG. 12. Effect of the plane echo eradication on the autospectrum for two gates on 15 December 1997 in an oblique beam. The left graph for each gate shows the fraction of contaminated points in the (8×128)-point-long period. The top and middle plots show the lowest frequency I component time series record before (top) and after (middle) the detection of the plane echo. The two bottom graphs show the plane parasited (left) and clean (right) autospectra.

15 December 1997. The left graph shows, as previously, the extent of the contamination along the vertical. The top graph shows the lowest frequency I component record, entire blocks discarded (dark gray and diagonal cross), or the contaminated points simply discarded (light gray). Note that for the purpose of the correlation computation, each time series block is detrended and recalibrated independently, yielding apparent steps at the transition between two blocks. The middle and bottom graphs show the correlation parameters without and with plane filtering, respectively. From left to right, the first graph depicts the autocorrelations versus time lag

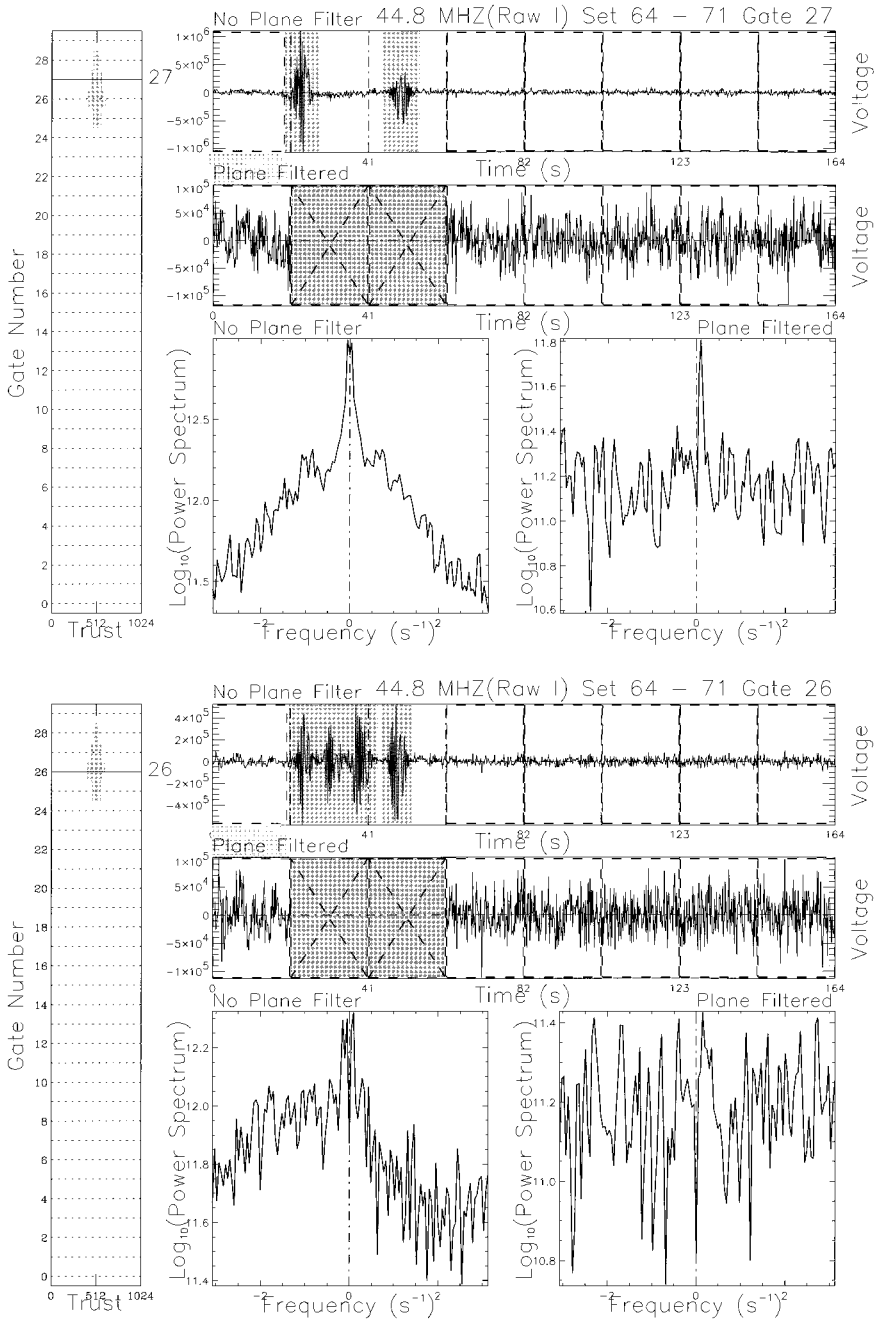

FIG. 13. Same as Fig. 12 but on 20 August 1996 and in a vertical beam.

for both frequencies (solid), their mean (dash and cross), their fits (dash–dot), and the domain used for the fits (hatching). The second graph depicts the cross-correlation normalized (solid) and nonnormalized (dash) modules. The last graph depicts the cross-correlation phase. Here the plane echo overlaps both integration periods. For the first one (top), an entire block has been discarded, whereas for the second one (bottom), only polluted points are discarded. In both cases, the correlation parameters are much smoother when the effect of the plane echo is removed and the FDI information is more detectable. The signal-to-noise ratio is deduced from the correlation analysis using the autocorrelations and their fits. The smoothness of the autocorrelations ensures more trustworthy signal-to-noise ratios.

The parameters of the plane filter module in the FDI processing chain are given here as illustrations. The processing environment allows a menu-oriented setup of those parameters, the graphic illustration of the module results, and the possibility to rerun the module after

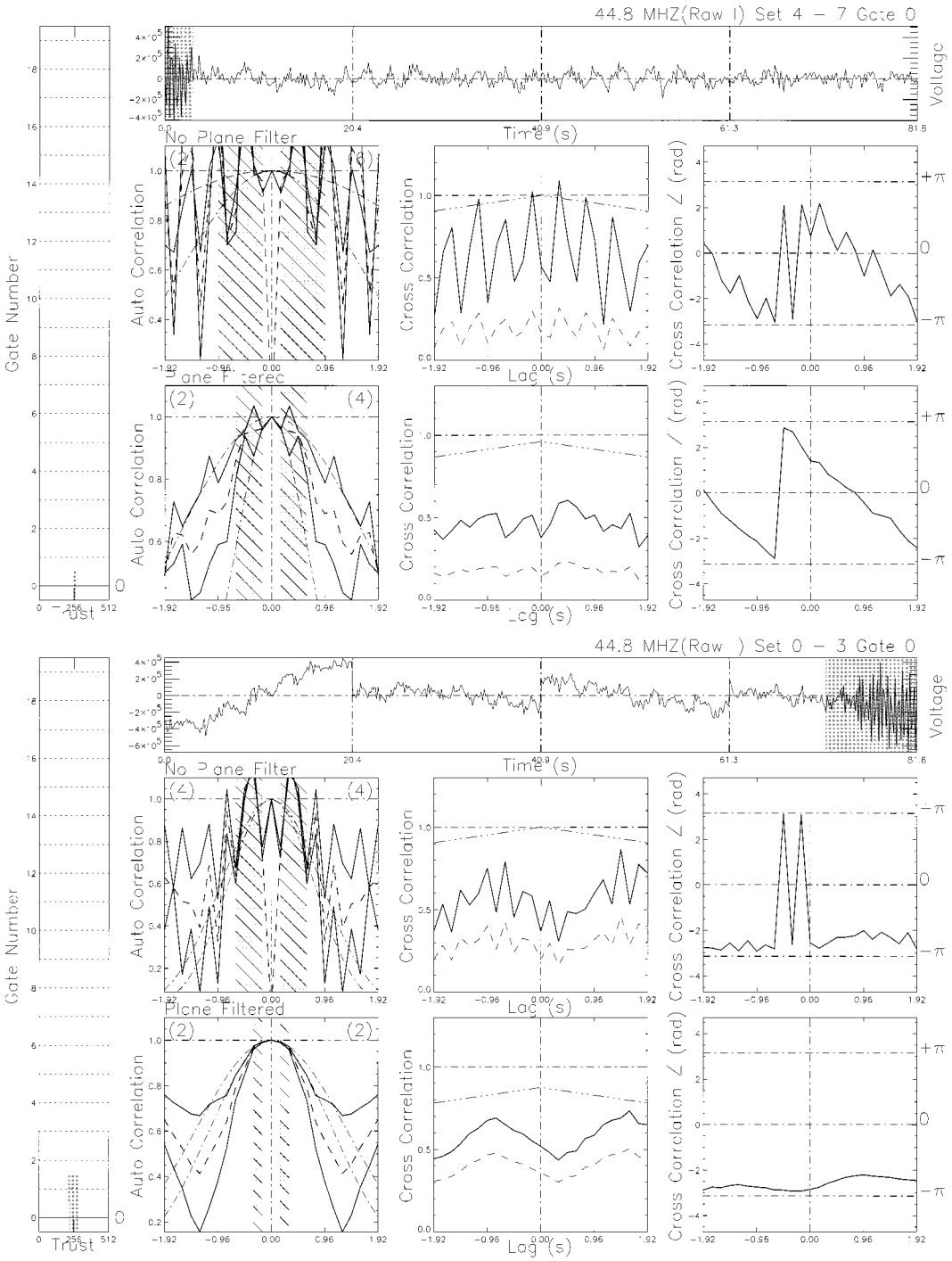

FIG. 14. Effect of the plane echo eradication on two consecutive (4×128)-point-long integration periods of the correlation parameters for a single gate on 15 December 1997 in an oblique beam. The left graph for each gate shows the fraction of contaminated points in the period. The top graph shows the lowest frequency I component time series record. The times discarded from the computation are shaded in gray. The middle and bottom rows show the correlation parameters before and after the plane detection, respectively. For each row, the left graph depicts both autocorrelations vs the time lag (solid), their mean (cross and dash), their fits (dash–dot), and the fit domain (hatching). The second graph shows the normalized (solid) and nonnormalized (dash) cross-correlation modules. The right graph shows the cross-correlation phase.

correcting the setup. This flexibility is necessary for the adaptation of the parameters to the current dataset. It also proved useful to correct the analysis when other parasites, such as strong voltage spikes, go through the crucible of the simulated wavelet analysis as potential plane echoes. Other than this, which is now prevented by a prior parasite filter module, the only observed caveat of this ''sped-up'' technique is the drift of the reference value coefficients. These coefficients are updated in the absence of a plane echo with the minimum over 20 wavelet coefficients, instead of the minimum over all 128 coefficients. A force reset of those reference values is allowed by the FDI processing. While rerunning the plane filter module, the first three blocks encountered in the current eight-block period are fully analyzed and the reference values are properly reset.

8. Conclusions

The wavelet filtering method presented in this paper can efficiently remove aircraft echoes appearing in ST radar measurements through a time series processing including convolution with two wavelet functions identified as levels 4 and 8, respectively, from a mother wavelet. This mother wavelet is inspired from the general signature of aircraft echoes on the time series.

The processing time of this wavelet filtering can be compared with the classic FFT. For a time series of N points, the FFT requires roughly (Lifermann 1976) $N \log_2 N$ operations. The wavelet transform uses the numerical expression deduced from (1), in which each integral is calculated by the finite differences method once at the beginning of the processing. For each wavelet transform defined by parameters a and b, we obtain $N + 1$ multiplications and $N - 1$ additions, respectively—that is, $2N$ operations to be considered for each point of the time series—so we obtain almost $40N$ operations, considering only the 20 largest absolute values of voltage to be sufficient for an effective airplane echo determination.

Using two wavelet transforms of level 4 and 8, as has been described previously, we finally obtain $80N$ operations. To get a more precise idea of the extra computation required, for 128 FFT points, the ratio is 11.4 (10 240 compared to 896 operations), and for 256 points, it becomes 10 (20 480 compared to 2048 operations). For classic VHF radars typically providing a 50-range-gate profile of 128 or 256 FFT points spectra every 10 s, this could be handled without difficulty, given the current processing capabilities of computers. Although this processing is about 10 times longer than the classic FFT for a 128- or 256-point record, it allows real-time implementation for VHF radars.

Thus, wavelet filtering represents a simple and efficient method for improving the quality of automatic measurements made by ST radars. It is used currently in a systematic way at CNRM on a workstation computer for a preliminary time series filtering before further studies of the radar signals, such as frequency domain interferometry, are performed.

REFERENCES

Balsley, B. B., and K. S. Gage, 1980: The MST radar technique: Potential for middle atmospheric studies. *J. Pure Appl. Geophys.*, **118,** 452–493.

Balsley, B. B., and K. S. Gage, 1982: On the use of ST radars for operational wind profiling. *Bull. Amer. Meteor. Soc.*, **63,** 1009–1018.

Daubechies, I., 1988: Orthonormal bases of compactly supported wavelets. *Commun. Pure Appl. Math.*, **41,** 909–996.

Jordan, J. R., and R. J. Lataitis, 1997: Removing ground and intermittent clutter contamination from wind profiler signals using wavelet transforms. *J. Atmos. Oceanic Technol.*, **14,** 1280–1297.

Klaus, V., 1988: Le profileur de vent (Radar Strato-tropospherique), applications à la météorologie opérationnelle. *La Meteorologie 7ème Ser.*, **21,** 19–29.

Larsen, M. F., 1983: The MST radar technique: Requirements for operational weather forecasting. *Handb. MAP*, **9,** 250–255.

——, and J. Röttger, 1982: VHF and UHF Doppler radars as tools for synoptic research. *Bull. Amer. Meteor. Soc.*, **63,** 996–1008.

Lifermann, 1980: *Les Méthodes Rapides de Transformation du Signal*. Masson, 197 pp.

Liu, P. C., and G. S. Miller, 1996: Wavelet transforms and ocean current data analysis. *J. Atmos. Oceanic Technol.*, **13,** 1090–1099.

Newland, D. E., 1994: Wavelet analysis of vibration, Part 1: Theory. *J. Vibration Acoust.*, **116,** 409–416.

Petitdidier, M., and Coauthors, 1990: The 961/45 MHz bifrequency INSU/Météo Stratospheric–Tropospheric radar. *Meteor. Rundsch.*, **42,** 142–151.

Strang, G., and T. Nguyen, 1996: *Wavelets and Filter Banks*. Wellesley-Cambridge Press, 490 pp.

Weng, H. Y., and K. M. Lau, 1994: Wavelets, period doubling, and time–frequency localization with application to organization of convection over the tropical western Pacific. *J. Atmos. Sci.*, **51,** 2523–2541.